Robotica: (2021) volume 39, pp. 1560–1574. © The Author(s), 2021. Published by Cambridge University Press.
doi:10.1017/S0263574720001356

Position-Based Fractional-Order Impedance Control of a 2 DOF Serial Manipulator

Selçuk Kizir* and Ali Elşavi

Department of Mechatronics Engineering, Kocaeli University, Umuttepe Campus, 41380, Kocaeli, Turkey
E-mail: ali-sh90@hotmail.com

(Accepted December 9, 2020. First published online: January 13, 2021)

SUMMARY
Impedance control is one of the interaction and force control methods that has been widely applied in the research of robotics. In this paper, a new position-based fractional-order impedance control scheme is proposed and applied to a 2 DOF serial manipulator. An RR robot manipulator with full arm dynamics and its environment were designed using Matlab/Simulink. The position control of the manipulator was utilized based on computed torque control to cancel out the nonlinearities existing on the dynamic model of the robot. Parameters of classical impedance controller (CIC) and proposed fractional-order impedance controller (FOIC) were optimized in order to minimize impact forces for comparison of the results in three conditions. In CIC condition: three constant parameters of the impedance controller were optimized: in Frac_λμ condition: Only non-integer parameters of the FOIC were re-optimized after the parameters in CIC had been accepted, and in Frac_all condition: all parameters of the FOIC were re-optimized. In order to show the effectiveness of the proposed method, simulations were conducted for all cases and performance indices were computed for the interaction forces. Results showed that impacts were reduced with an improvement of 26.12% from CIC to Frac_λμ and an improvement of 47.21% from CIC to Frac_all. The proposed scheme improves the impedance behavior and robustness showing better impact absorption performance, which is needed in many challenging robotic tasks and intelligent mechatronic devices.

KEYWORDS: Fractional-order control; Impedance control; Computed torque control; Robot manipulator; Optimization.

1. Introduction

Nowadays, robots are being used widely more and more in assembly operations, medical, home applications, services, defense, space exploration etc., where contact environment cannot be modeled accurately.[1] Most of these robots need object manipulation, and they are also started to work with humans in shared workspace. Therefore, an interaction control (compliance) method is necessary for the robot manipulator to interact with an unknown environment safely and human-friendly, avoiding damages in both the environment and the robot itself. When a robot is contacted with an unclear environment, impedance or force control can be utilized to control the interaction between the robot and its environment. The fundamental difference between the two approaches is that the force control attempts to follow a specific reference of the contact force, while impedance control[2] aims to realize a good dynamic relation between position of the end-effector and contact force.[3] The fundamental philosophy of the impedance control, according to Hogan,[4] is that the manipulator control system should be designed not to track a motion trajectory alone, but rather to regulate the mechanical impedance of the manipulator. Impedance control can be implemented as position-based (outer

* Corresponding author. E-mail: selcuk.kizir@kocaeli.edu.tr

force loop) or force-based (inner force loop) approaches in the literature. Position-based impedance control method is an appropriate and feasible method for robotic systems which has traditional position controller in order to provide interaction and force requirements. Impedance control method is used in different fields, such as robots which are able to move and carry sensitive things without any damage, human–robot interaction,[5–6] industrial robots used in vehicle assembly operations,[7] microscale working robots,[8] and surgical robots.[9]

In addition, most of the real dynamic systems are better represented by a non-integer-order dynamic model using fractional calculus of integration and/or differentiation of non-integer order. Fractional calculus is a topic of a more than 300-year-old start with the French mathematician Gottfried Wilhelm Leibnitz. The number of applications related to fractional calculus is rapidly growing. Many researchers have done works in different areas of engineering and science using fractional calculus.[10–12] Fractional calculus can be utilized in three different forms in the control applications such that: (i) fractional-order controller and integer-order plant, (ii) integer-order controller and fractional-order plant, and (iii) fractional-order controller and fractional-order plant.[13] Using a fractional-order controller provides more flexibility in tuning gain and phase characteristics of a system. This allows to design alternative robust control systems which requires much less controller tuning parameters.[13] The main concept of fractional calculus has a massive potential to change the way of the model and control of the world seen around us, where all objects are generally fractional.[14] Controllers using fractional-order derivatives and integrals have been extensively used by many scientists in robotic manipulators,[15] mechatronics systems,[16] system identification,[17] and physical systems whose behavior can be controlled with fractional-order proportional-integral-derivative controllers.[18–19]

In this paper, we have proposed a new position-based fractional-order impedance controller (FOIC) in order to achieve a wider control workspace on the interaction problems. There is just three related work with the fractional impedance control that has been done previously according to literature reviews.[20–22] Oh and Hori[20] suggested force sensor-less fractional impedance control first in 2008. They proposed a new discretization method of fractional integrator using the particle swarm optimization method. They presented experimental results of a one link robot arm that providing impedance control in a wide frequency range. However, they applied fractional-order calculus to only integral part of the impedance controller and do not consider derivative term of the impedance controller. Kobayashi and others[21] proposed a novel first-order impedance control using fractional calculation inspired by material properties of muscle. They reported that their new controller showed good impact absorption, especially for assistive and rehabilitation robots. However, they applied fractional-order calculus to only derivative part of the impedance controller and do not consider integral term of the impedance controller. Chen et al.[22] applied second-order fractional-order impedance control to wheel hexapod legged robot for solving ground impacts. They presented simulation results of the one DOF actuator control system which provides compliance and handles the impacts. Our study is the first study which analyzes the impact effects of integer and non-integer impedance control of a serial manipulator. This new controller will be tested on a 2 DOF serial manipulator under different conditions where parameters of the classical impedance controller (CIC) and novel FOIC were optimized to achieve the most robust performance. Stability conditions of the FOIC were also analyzed. This paper is structured as follows: Section 2 reviews the system modeling and control which contains the mechanical and dynamic model that was designed and modeled in SimMehanics/Matlab, and position controller based on computed torque control. In Section 3, the environment and contact forces that acting on the robot manipulator would definitively change its dynamic behavior were discussed. The proposed fractional-order impedance control scheme was presented in Section 4. The simulation results were presented in Section 5 to demonstrate the efficiency of the proposed scheme for the CIC, Frac_λμ (FOIC – only non-integer parameters optimized) and Frac_all (FOIC – all parameters optimized), and for the changing of the environmental parameters.

2. System Modeling and Control

2.1. Mechanical and dynamic model

First step is to develop a model of a 2 DOF robot manipulator to test our new proposed controller. Figure 1 shows the mechanical model and coordinate systems of the robot manipulator, that it is

https://doi.org/10.1017/S0263574720001356 Published online by Cambridge University Press

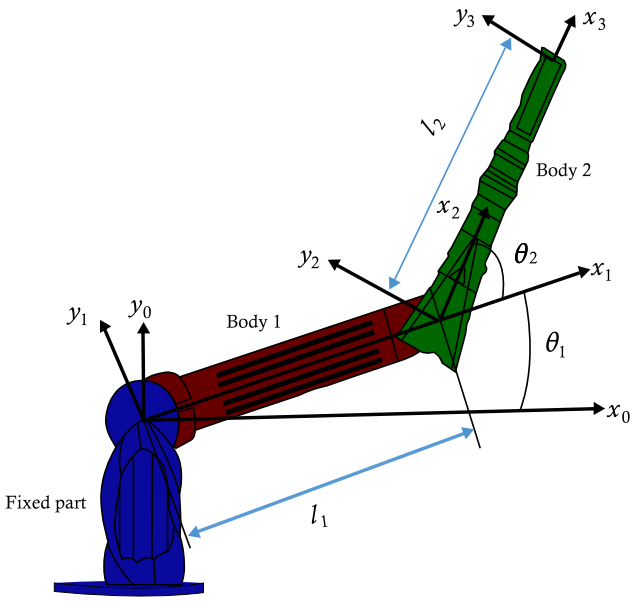

Fig. 1. Coordinate systems of 2 DOF Robot manipulator.

designed in SimMechanics/Matlab. The model consisted of fixed part, two bodies and two revolute joints. The model receives torques as input in joint space, and the outputs are end-effector position in Cartesian coordinates and joint angles.

Dynamics of a robot manipulator is explicitly derived based on the Lagrange–Euler formulation to explain the problems involved in dynamic modeling, that the dynamic model relates the forces acting on the mechanical structure with the resulting displacement, velocities, and accelerations.[23] Here, these forces can be arisen from different sources like the inertia of the mechanical links, the torques generated by the motors, the friction forces, and the possible forces exerted from the environment on the robot. The arm mechanism was considered as an open kinematic-chain combination. Forward kinematics of the robot manipulator is derived using the formulation by Denavit Hartenberg convention. Then, by using the Lagrange equation, we get the dynamics model of the system. Actuator dynamics (motors and gearboxes) and friction forces are ignored in this model. In addition, it is assumed that the robot is rigid and there is no flexibility in joints. Since it is a simple model, the inertial matrix (I) is accepted as zero in the dynamic equation. In Matlab/Simulink simulation environment, the inertial matrix of the model is calculated on the SimMechanics interface and applied to the system.

The dynamic equations for the robot manipulator are usually presented by the coupled non-linear differential equation that was derived from the Lagrangian method.[23]

$$M(\theta)\,\ddot{\theta} + C\left(\theta, \dot{\theta}\right) + G(\theta) = u \tag{1}$$

where θ is the joint variable and u is the vector of generalized forces applied to the robot manipulator. $M(\theta)$ is the inertia matrix of the manipulator, $C\left(\theta, \dot{\theta}\right)$ is the vector of centripetal and Corilios, and $G(\theta)$ is the gravity vector. The dynamic model following the Lagrangian formulation for the 2 DOF robot manipulator is:

$$M(\theta)\begin{bmatrix}\ddot{\theta}_1\\ \ddot{\theta}_2\end{bmatrix} + C\left(\theta, \dot{\theta}\right) + G(\theta) = \begin{bmatrix}u_1\\ u_2\end{bmatrix} \tag{2}$$

where

$$M(\theta) = \begin{bmatrix}(m_1+m_2){l_1}^2 + m_2{l_2}^2 + 2m_2l_1l_2\cos\theta_2 & m_2{l_2}^2 + m_2l_1l_2\cos\theta_2\\ m_2{l_2}^2 + m_2l_1l_2\cos\theta_2 & m_2{l_2}^2\end{bmatrix} \tag{3}$$

https://doi.org/10.1017/S0263574720001356 Published online by Cambridge University Press

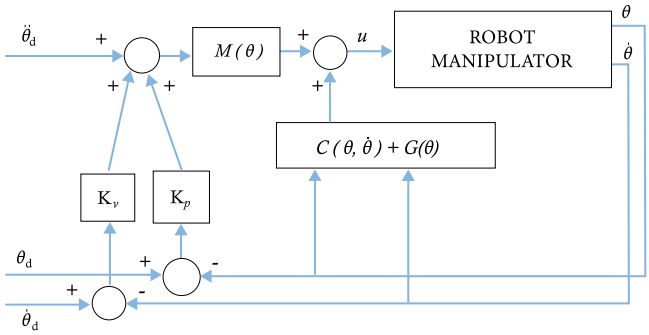

Fig. 2. Computed torque control scheme.

$$C\left(\theta, \dot{\theta}\right) = \begin{bmatrix} -m_2 l_1 l_2 \left(2\dot{\theta}_1 \dot{\theta}_2 + \dot{\theta}_2^2\right) \sin\theta_2 \\ m_2 l_1 l_2 \dot{\theta}_1^2 \sin\theta_2 \end{bmatrix} \tag{4}$$

$$G(\theta) = \begin{bmatrix} (m_1 + m_2) g l_1 \cos\theta_1 + m_2 g l_2 \cos(\theta_1 + \theta_2) \\ m_2 g l_2 \cos(\theta_1 + \theta_2) \end{bmatrix} \tag{5}$$

The terms l_1 and l_2 are the lengths of link 1 and 2 and m_1, m_2 are their masses, respectively. In this work, $l_1 = l_2 = 0.16$ m and $m_1 = m_2 = 1$ kg for simplicity.

2.2. Position control

The dynamic model of the manipulator is nonlinear and highly coupled. Computed torque controller is used to control the position of the robot end-effector. The computed torque method is an effective motion control strategy for robotic manipulator systems, which is a significant nonlinear controller for certain systems that is depended on feedback linearization. It computes the required joint torques by using the nonlinear feedback control law. Figure 2 shows the configuration of the computed torque scheme.

$$u = M(\theta)\left[\ddot{\theta}_d + K_v \dot{e} + K_P\, e\,\right] + C\left(\theta, \dot{\theta}\right) + G(\theta) \tag{6}$$

The control law in (6) represents the standard structure of the computed torque control strategy. $\ddot{\theta}_d$, $\dot{\theta}_d$, and θ_d are the vector of desired acceleration, velocity, and position, respectively, in (6). The joint position error is denoted by the vector $e = \theta_d - \theta$, while $\dot{e} = \dot{\theta}_d - \dot{\theta}$ is the vector of velocity error.The computed torque control in (6) has two parameters, K_p and K_v which are the proportional and derivative gains ($K_p = 4000$, $K_v = 2000$), respectively. The parameters of the torque control were optimized in the simulation environment which were tuned with the help of the Control System Tuner.

In most of the industrial manipulators, possibility of sending torque commands to the robot directly is not available. Therefore, by using the inverse kinematics algorithms, it became possible to send direct joint angle commands to the robot or end-effector position or orientation command in Cartesian coordinates.[23] The possible solutions for θ_1 and θ_2 angles of robotic arm can be written as in (7) and (8).

$$\Theta_2 = A\tan2\left(\pm\sqrt{1 - \left[\frac{P_x^2 + P_y^2 - l_1^2 - l_2^2}{2 l_1 l_2}\right]^2}, \frac{P_x^2 + P_y^2 - l_1^2 - l_2^2}{2 l_1 l_2}\right) \tag{7}$$

$$\theta_1 = A\tan2\left(P_y\,,\, P_x\right) \pm A\tan2\left(\sqrt{P_y^2 + P_x^2 - \left(l_2\cos\theta_2 + l_1\right)^2}, l_2\cos\theta_2 + l_1\right) \tag{8}$$

where P_y, P_x are the end-effector position, and l_1 and l_2 are the lengths of the first and second link, respectively. The mathematical solution does not always represent the physical solution. According to the resulting solution sets, four different positions of the robot's end-effector were found. The

https://doi.org/10.1017/S0263574720001356 Published online by Cambridge University Press

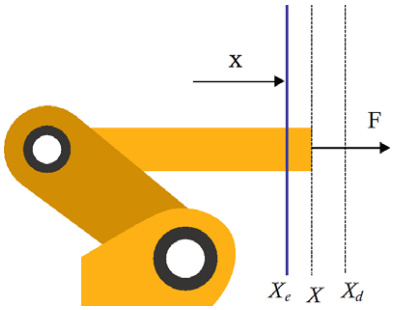

Fig. 3. The contact between robot and environment.

possible solutions help the robot to reach the correct position in multiple configurations. The positive solutions of θ_1 and θ_2 have been chosen by placing them in the position vector in the forward kinematics and used in the model. In order to obtain the results of this work in an easy and useful way, the mechanical model, the computed torque controller, and the inverse kinematics of manipulator can be integrated into one block, which represents the robot manipulator.

3. The Environment and Contact forces

The dynamic model does not take into account possible external forces acting on the robot, which may change the dynamic behavior of the robot manipulator. Therefore, a model of the environment will be included in the system. The environment's model is used as a linear spring with constant K_e generally, but to cover a large range of environments, we will include a damping coefficient with the spring,[24] that the environment can take several models to describe the dynamics of objects. The environment is modeled as in (9).

$$f = K_e(X - X_e) + B_e(\dot{X} - \dot{X}_e) \tag{9}$$

where K_e is the stiffness of the environment, B_e is the damping coefficient of the environment, f is the contact force, X_e is the static position of the environment, and X is the end-effector position at the contact point. Figure 3 shows the interaction between the robot and the object, where the robot is trying to reach the desired position X_d and colliding with the environment at position X_e.

Then, to make the system closer to a real and clearer, Eq. (1) was modified to show the effect of those forces that the dynamic equation could be defined as in (10).

$$M(\theta)\ddot{\theta} + C\left(\theta, \dot{\theta}\right) + G(\theta) = u - J^T(\theta)f \tag{10}$$

The term $J^T(\theta)f$ translates the task-space forces to the joint. The relation between forces and torques is defined as in (11).

$$\tau_c = J^T(\theta)f \tag{11}$$

where τ_c is the contact torques, J^T is the transpose of a Jacobian matrix. The Jacobian matrix Eq. (12) is shown as follows:

$$J(\theta) = \begin{bmatrix} J_v(\theta) \\ J_w(\theta) \end{bmatrix} = \begin{bmatrix} -l_1 s\theta_1 - l_2 s\theta_1\theta_2 & -l_2 s\theta_1\theta_2 \\ l_1 c\theta_1 + l_2 c\theta_1\theta_2 & l_2 c\theta_1\theta_2 \\ 0 & 0 \\ 0 & 0 \\ 0 & 0 \\ 0 & 1 \end{bmatrix} \tag{12}$$

where J_v and J_w are linear and angular velocity of the end-effector, respectively. In this work, we consider a two-dimensional case, in which the contact force acts over X and Y axes.

https://doi.org/10.1017/S0263574720001356 Published online by Cambridge University Press

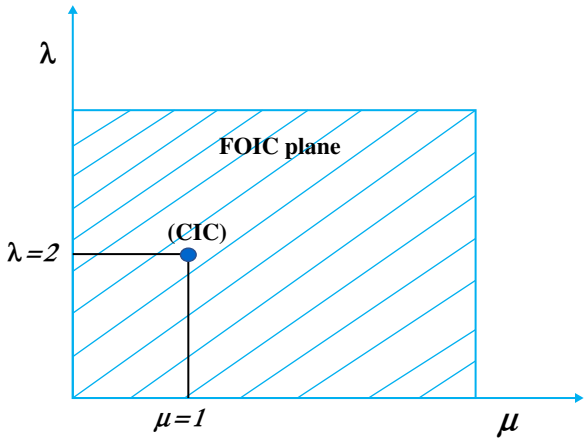

Fig. 4. Fractional-order impedance controller plane.

4. Fractional-Order Impedance Controller

When the robot follows a trajectory and suddenly an object or obstacle appears on its path, end-effector will collide with it and also trying to reach the final desired position of the trajectory, and applying an impact force into the environment.[23] This scenario might cause damages to the robot or to objects. Therefore, the impedance control which is one of the interaction methods is used widely in these issues in which the input of the impedance controller is the impact forces. The measured contact forces are feedback to the impedance controller, and output of the impedance controller will be a modified robot trajectory. That means if the forces are not sensed, the trajectory would be followed accurately. Otherwise, the trajectory will be modified in order to regulate the maximum forces. Equation (13) gives the control law of the traditional position-based impedance controller,[25] which represents a virtual mass-spring-damper system between the robot and the object.

$$M_t\ddot{e}_t + D_t\dot{e}_t + K_t e_t = f \tag{13}$$

where M_t, D_t, and K_t are the inertia, damping, and the stiffness coefficients, respectively, $e_t = (x_d - x_m)$ is the trajectory error where x_d is the desired input trajectory and x_m is the modified trajectory. In this paper, a new position-based FOIC will be proposed. A FOIC is an extension of the CIC. Robustness of the fractional-order controllers is better, and they are less sensitive to parameter uncertainties.[19] The differential equation of the FOIC is given as follows:

$$M_t e(t)\Gamma^{\lambda} + D_t e(t)\Gamma^{\mu} + K_t e(t) = f(t) \tag{14}$$

where M_t, D_t, and K_t are the inertia, damping, and the stiffness coefficients, respectively, $e(t)$ is the trajectory error, Γ^{λ} and Γ^{μ} are the fractional-order differentiation, respectively. Theoretically, Eq. (14) is an infinite dimensional linear filter because of non-integer integral and derivative part.[13] The continuous transfer function of the FOIC is obtained by Laplace transformation, as given by (15):

$$G(s) = \left(M_t s^{\lambda} + D_t s^{\mu} + K_t\right)F(s) \tag{15}$$

where, $G(s)$ is the controller output, λ and μ is the order of differentiator, (λ, $\mu = 0$). Non-integer toolbox[26] was used for the fractional calculus in this study.

The CIC is particular case of the fractional controller, where λ is equal to two and μ is equal to one as shown on Fig. 4. Therefore, we also have to tune two more parameters, the order of fractional derivatives λ and μ, in addition to tuning the CIC constants M_t, D_t, and K_t. This means that the FOIC can be represented by a plane where the CIC is a single fixed point. It is possible to tune control parameters continuously in this larger plane, where λ and μ has an infinite number of values that give a wide range of freedom to represent the dynamic and control systems very close to the real systems and in order to obtain high-performance system.

https://doi.org/10.1017/S0263574720001356 Published online by Cambridge University Press

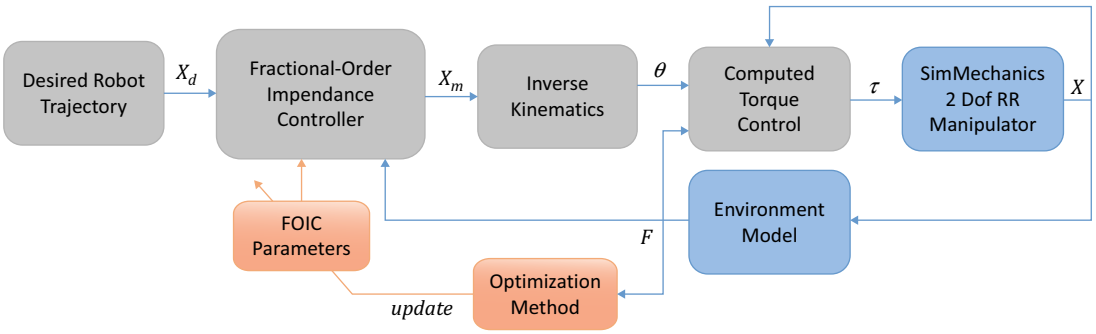

Fig. 5. Simplified block diagram of the proposed fractional-order impedance control scheme.

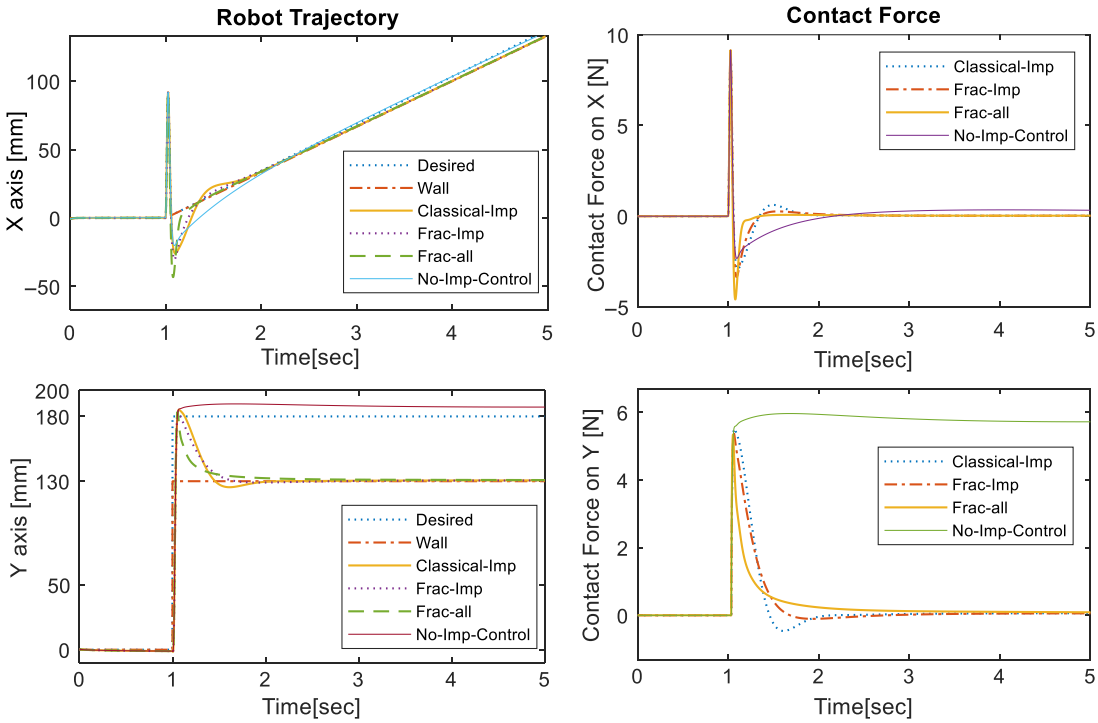

Fig. 6. Robot trajectory (left) and response of contact force (right). $(Y_e, Y_d) =$ (130, 180) mm, $K_e =$ 100 N/m.

5. Optimization of the Fractional-Order Impedance Controller

In this section, the optimization algorithm used for the CIC and FOIC parameters and the obtained results after several experiments will be presented and discussed. From Eq. (15), five parameters (M_t, D_t, K_t, λ, and μ) are required to be optimized. Tuning of five parameters is a challenging work, so a direct optimization method which is based on the Nelder-Mead also known as simplex search algorithm is utilized for fair comparison. Simplex search optimization algorithm[27] was used to optimize the required parameters to minimize the contact forces equal to zero in order to get safe contact without any damage to the robot and environment.

Figure 5 shows a simplified block diagram of the robot manipulator and the proposed controller in this paper, after designing and modeling the all components of them as discussed above. It contains the mechanical model and inverse kinematics of the robot manipulator, the position controller, the model of the environment, and the proposed FOIC.

Optimization was made based on Fig. 6 where a ramp and step signals on X-axis and Y-axis were applied for the desired trajectories. This means that manipulator end-effector firstly hits to a wall then slides on the wall. For comparison of the results of CIC and proposed FOIC, we have three cases: (i) CIC, (ii) Frac_$\lambda\mu$ (FOIC with optimized only λ and μ) and (iii) Frac_all (FOIC with optimized all parameters). Only red parameters were optimized of the CIC and FOIC in Tables I, II and III.

https://doi.org/10.1017/S0263574720001356 Published online by Cambridge University Press

Table I. Controller parameters in CIC.

CIC		
Controller parameters	**Value**	**Unit**
M_t	1.5098	Kg
D_t	20.1504	Ns/m
K_t	1.2485	N/m
λ	2	–
μ	1	–

Table II. Controller parameters in Frac_λμ.

Frac_λμ		
Controller parameters	**Value**	**Unit**
M_t	1.5098	Kg
D_t	20.1504	Ns/m
K_t	1.2485	N/m
λ	1.2803	–
μ	1.0099	–

Table III. Controller parameters in Frac_all.

Frac_all		
Controller parameters	**Value**	**Unit**
M_t	0.0019	Kg
D_t	17.2355	Ns/m
K_t	0.0015	N/m
λ	0.3322	–
μ	0.7462	–

In Frac_λμ case, we kept the previous values of the CIC of the first case and we only have optimized the proposed FOIC's non-integer parameters λ and μ in order to study the effect of using the fractional control algorithm on the model results. In Frac_all case, we have optimized all parameters of the FOIC together.

Figure 6 shows the position trajectories and the contact forces between the robot manipulator and the environment for the three cases. The robot hits a flat wall placed at $Y_e = 130$ mm on axis Y and then follows a trajectory by sliding on axis X when the step trajectory was applied as desired trajectory ($Y_d = 180$ mm). The environment stiffness K_e and the environment damping B_e are ($K_e = 100$ N/m, $B_e = 0.1$ Ns/m) in this simulation. We note that, the contact force is rising on both axes rapidly at the contact at $t = 1$ s. However, the controller regulates the trajectory with the new environment with contact force equal to zero, depending on the controller parameters, which were optimized. The force seen on axis X was resulted from the hit on axis Y because of the disturbance by $\tau_c = J^T(\theta) f$. Also, Fig. 6 shows the results if no impedance controller was utilized for clear understanding of the interaction behavior. Figure 7 shows the control signals for the motion in Fig. 6. It can be seen from the figure that Frac_all was responded faster than others, while amplitudes of the signals were in the same limits.

https://doi.org/10.1017/S0263574720001356 Published online by Cambridge University Press

Table IV. Contact force errors RMSE, MSE, and MAE, K_e =100 N/m.

	RMSE		MSE		MAE	
***Ke* = 100 N/m**	***X***	***Y***	***X***	***Y***	***X***	***Y***
CIC	0.7838	0.9919	0.6144	0.9839	0.2099	0.2966
Frac_λμ	0.7530	0.8866	0.5670	0.7861	0.1828	0.2664
Frac_all	**0.7355**	**0.6270**	**0.5409**	**0.3932**	**0.1412**	**0.2542**

MSE, mean squared error; MAE, mean absolute error.

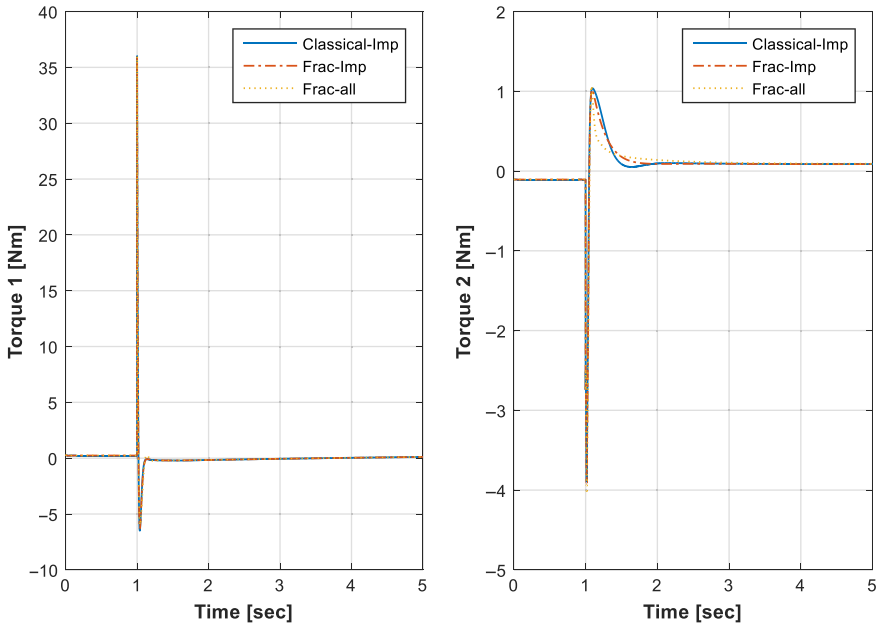

Fig. 7. Joint torques for the motion in Fig. 6. $(Y_e, Y_d) =$ (130, 180) mm, $K_e = 100$ N/m.

In addition, root-mean-squared error (RMSE), mean squared error, and mean absolute error were utilized for calculating the contact force errors in order to analyze the control performances of the CIC, Frac_λμ, and Frac_all. These indices were defined in Eq. (16).

$$\mathbf{RMSE} = \sqrt{\frac{1}{N}\sum_{i=1}^{N}(e(t))^2},\ \mathbf{MSE} = \frac{1}{N}\sum_{i=1}^{N}(e(t))^2,\ \mathbf{MAE} = \frac{1}{N}\sum_{i=1}^{N}|e(t)| \tag{16}$$

Results from Table IV showed that an improvement of 4% on X-axis and 10.31% on Y-axis was achieved from the CIC to Frac_λμ according to RMSE. Also, an improvement of 6.16% on X-axis and 36.7% on Y-axis was achieved in Frac_all in comparison to CIC. The best results are illustrated using bold text in the tables.

5.1. Robustness tests

A variety of real physical phenomena are represented by fractional-order differential equations and, thus, fractional-order transfer functions. Successful modeling of fractional-order systems at the Matlab/Simulink is dependent by the possibility of their integer-order approximation. CRONE approximation was applied on the transfer function of FOIC, which is given previously in (15); this approximation utilizes a recursive distribution of N zeros and N poles leading to a transfer function as follows:

$$C(s) = k' \prod_{n=1}^{N} \frac{1 + \frac{s}{w_{zn}}}{1 + \frac{s}{w_{pn}}} \tag{17}$$

https://doi.org/10.1017/S0263574720001356 Published online by Cambridge University Press

where k'' is an adjusted gain. Zeros and poles are to be found within a frequency range $[w_h;w_l]$. The fractional-order transfer function after using the approximation for Frac_λμ and Frac_all given in (18) and (19), respectively.

$$C_{Frac\_\lambda\mu}(s) = \frac{1}{1.5918s^{1.2803} + 20.1504s^{1.0099} + 1.2485} \approx \frac{0.7692s^2 + 0.8922s + 0.2096}{17.1s^3 + 19.38s^2 + 5.141s + 0.2617} \tag{18}$$

$$C_{Frc\_all}(s) = \frac{1}{0.0019s^{0.3322} + 17.2355s^{0.7462} + 0.0015} \approx \frac{0.1664s^2 + 0.8583s + 0.6898}{12.27s^2 + 12.25s + 0.2949} \tag{19}$$

The FOIC can be represented by a well-known linear second-order system for stability analysis. The natural frequency and damping ratio of the second-order system are given below, respectively:

$$w_n = \sqrt{\frac{K_t}{M_t}} \tag{20}$$

$$\xi = \frac{D_t}{2M_t w_n} \tag{21}$$

The stability of the position-based classical impedance control was studied before, and the stability conditions are found by Eqs. (22), (23), and (24) according to geometric criterion,[28] H_{inf} geometric criterion,[28] and investigated by Benady,[29] respectively.

$$\xi > 0,5(\sqrt{1+k} - 1) \tag{22}$$

$$\xi > 0,5(\sqrt{1+2k} - 1) \tag{23}$$

$$\xi > \sqrt{1+k} \tag{24}$$

where $k = K_e/K_t \gg 1$ and K_e is the stiffness of the environment or object. After computing values according to the previous equations, we find that stability condition is satisfied by Eq. (23) (7.3383 > 5.8480) for CIC for $K_e = 100$. Stability is lost when environment stiffness K_e is more than 305.577, 152.788, and 65.984 for CIC, according to Eqs. (22)–(24), respectively.

Experiment was repeated as similar to the previous simulation (Fig. 6) but changing environment stiffness with $K_e = 200$ N/m to test the controller's performance with different environmental parameters. Figure 8 shows the position trajectories and the contact forces. The contact force values has increased due to the change in Ke value as in Eq. (9). Figure 9 shows the control signals for the motion in Fig. 8. Contact stability of an impedance controller can be defined as contacting with an environment without growing oscillations and without loss of contact.[28] Therefore, from this perspective, FOICs were shown more robust behavior than CIC. Stability of the CIC is lost when the environment stiffness is more than 152.788 according to Eq. (23), and it is observed that stability of the Frac_all was maintained up to $K_e = 250$ in this experiment.

Results from Table V showed that with $K_e = 200$ N/m, an improvement of 8.59% on X-axis and 21.81% on Y-axis was achieved from the CIC to Frac_λμ according to RMSE. Also, an improvement of 9.15% on X-axis and 46.17% on Y-axis was achieved in Frac_all in comparison to CIC.

In general cases, a wall is not flat and non-uniform; hence, the force tracking control should guarantee surface variation of the environment. For this reason, a triangular type of indent wall tracking experiment was conducted. In this simulation, when the step trajectory was applied as the desired trajectory ($Y_d = 180$ mm) to the CIC and proposed controller FOIC, the environment stiffness K_e and the environment damping B_e are exactly known (K_e= 100 N/m, B_e= 0.1 Ns/m). The results of this simulation are shown in Fig. 10 for the triangular type of indent wall. Figure 11 shows the control signals or joint torques for the motion in Fig. 10. The contact force is rising rapidly at the contact at $t = 1$ s; then, the controller quickly regulates the trajectory with contact force equal to zero.

Results from Table VI showed that an improvement of 6.22% on X-axis and 15.6% on Y-axis was achieved from the CIC to Frac_λμ according to RMSE. Also, an improvement of 7.16% on X-axis and 42.3% on Y-axis was achieved in Frac_all in comparison to CIC.

https://doi.org/10.1017/S0263574720001356 Published online by Cambridge University Press

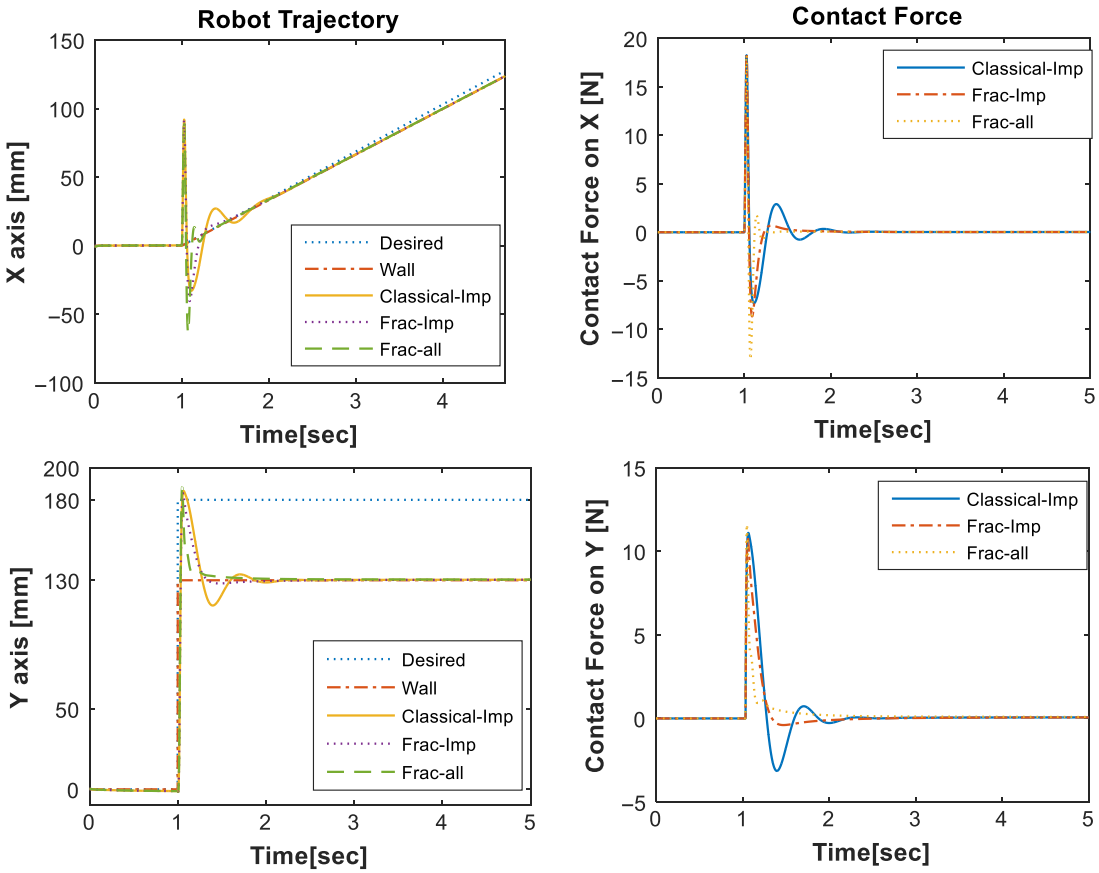

Fig. 8. Robot trajectory (left) and response of contact force (right). $(Y_e, Y_d) =$ (130, 180) mm, $K_e = 200$ N/m.

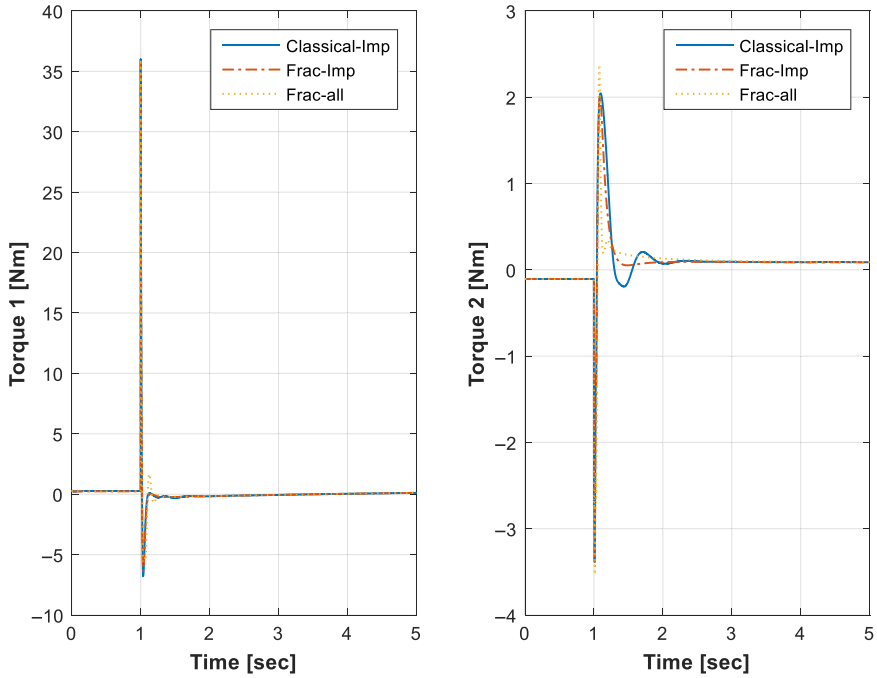

Fig. 9. Joint torques for the motion in Fig. 8. $(Y_e, Y_d) =$ (130, 180) mm, $K_e = 200$ N/m.

https://doi.org/10.1017/S0263574720001356 Published online by Cambridge University Press

Table V. Contact force errors RMSE, MSE, and MAE, K_e =200 N/m.

	RMSE		MSE		MAE	
***Ke* =200 N/m**	***X***	***Y***	***X***	***Y***	***X***	***Y***
CIC	1.7060	1.7224	2.9106	2.9666	0.4581	0.5015
Frac_λμ	1.5593	1.3467	2.4313	1.8137	0.3166	0.3180
Frac_all	**1.5498**	**0.9271**	**2.3120**	**0.8596**	**0.2561**	**0.2590**

MSE, mean squared error; MAE, mean absolute error.

Table VI. Contact force errors RMSE, MSE, and MAE, K_e =100 N/m.

	RMSE		MSE		MAE	
***Ke* =100 N/m**	***X***	***Y***	***X***	***Y***	***X***	***Y***
CIC	0.8653	0.9760	0.7456	0.9527	0.1723	0.3215
Frac_λμ	0.8114	0.8237	0.6584	0.6785	0.1392	0.2801
Frac_all	**0.8033**	**0.5634**	**0.6452**	**0.3174**	**0.1114**	**0.2151**

MSE, mean squared error; MAE, mean absolute error.

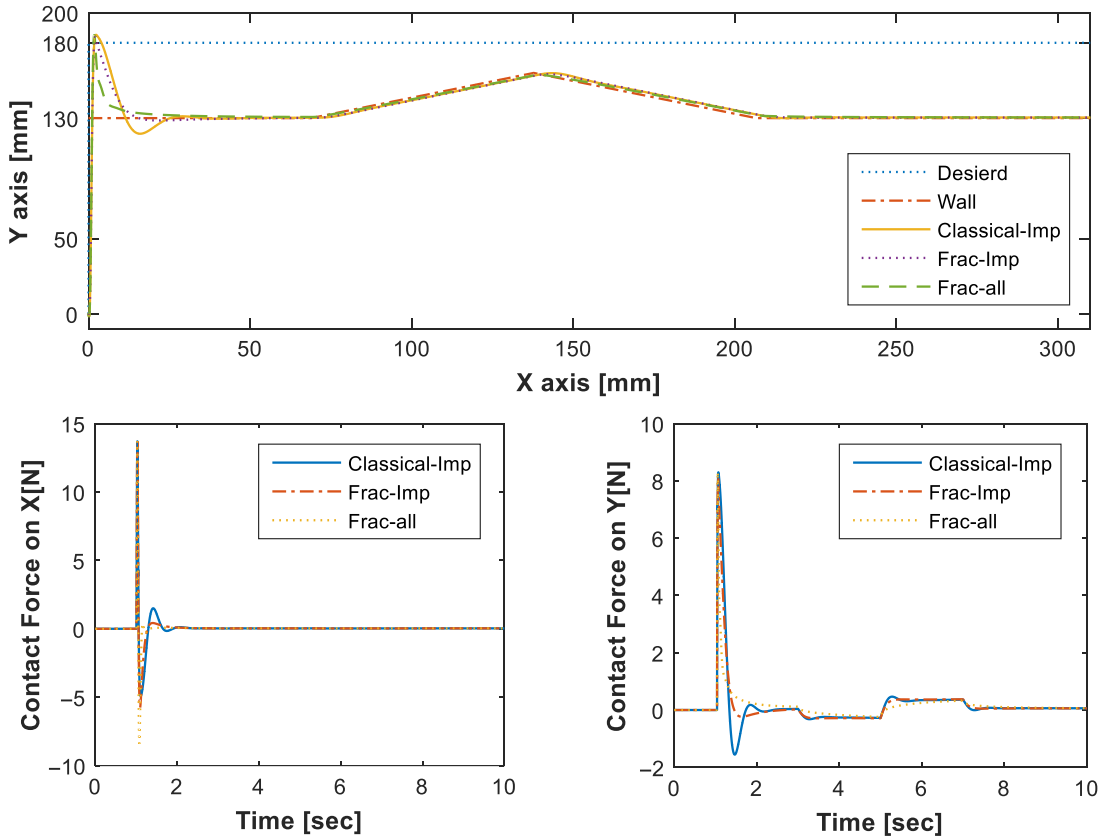

Fig. 10. Robot trajectory (left) and response of contact force (right). Y_d= 180 mm, K_e= 100 N/m.

Figure 12 shows the position trajectories and the contact forces similar to the previous simulation that the wall is not flat, but with environment stiffness $K_e = 200$ N/m. Figure 13 shows the control signals or joint torques for the motion in Fig. 12.

Results from Table VII showed that an improvement of 11.8% on X-axis and 26.12% on Y-axis was achieved from the CIC to Frac_λμ according to RMSE. Also, an improvement of 9.2% on

https://doi.org/10.1017/S0263574720001356 Published online by Cambridge University Press

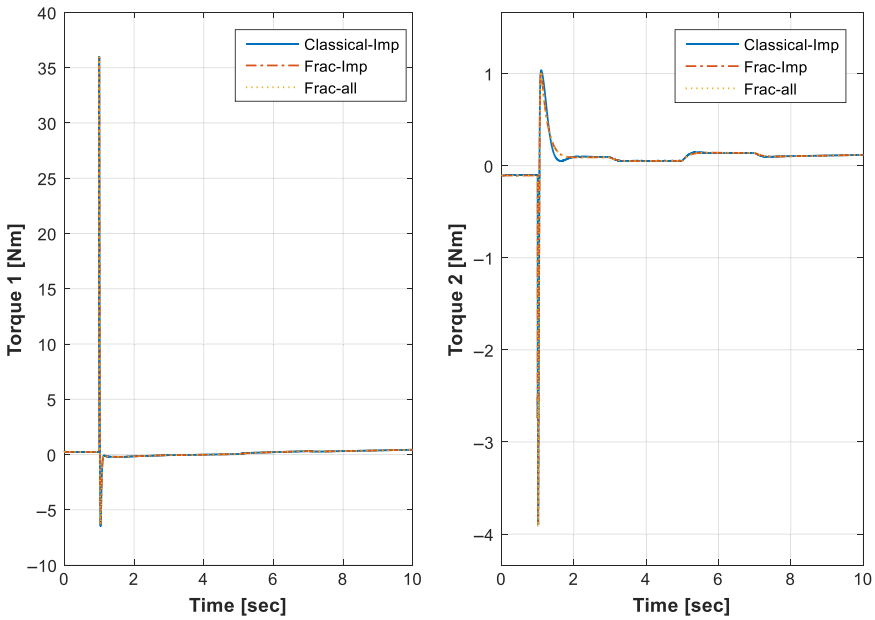

Fig. 11. Joint torques for the motion in Fig. 9. Y_d= 180 mm, K_e= 100 N/m.

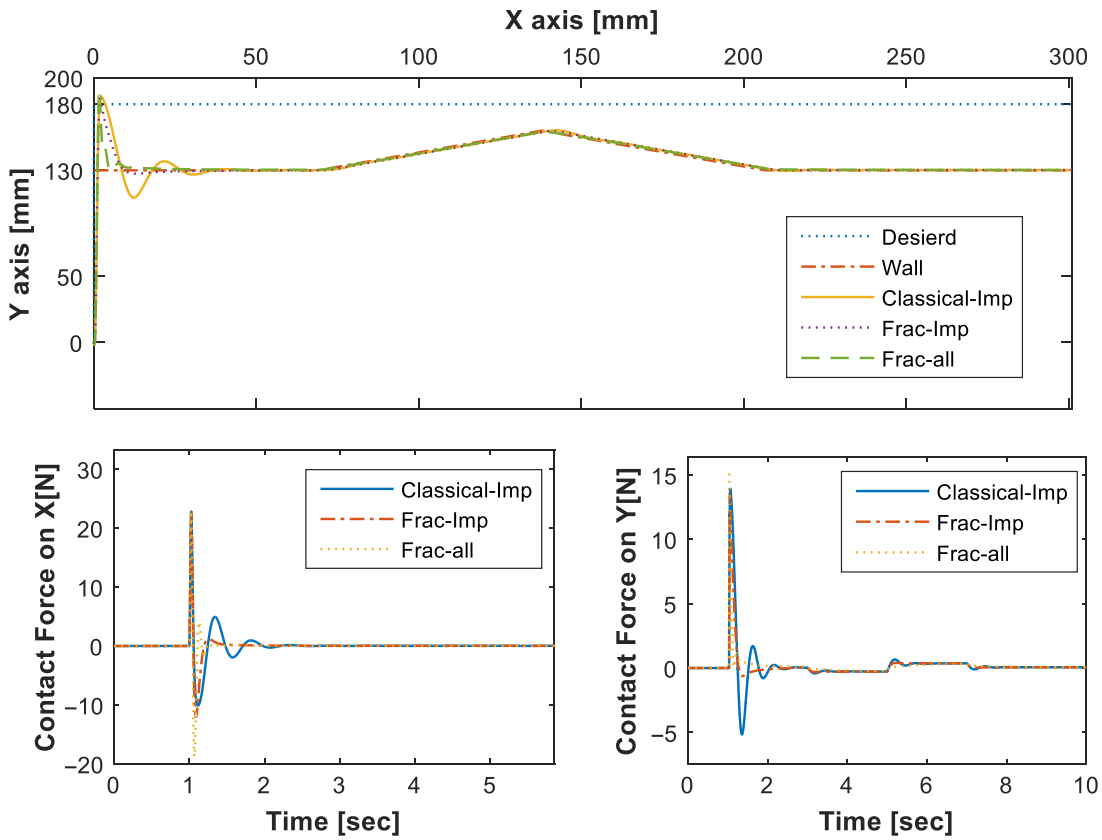

Fig. 12. Robot trajectory (left) and response of contact force (right). Y_d= 180 mm, K_e= 200 N/m.

X-axis and 47.21% on Y-axis was achieved in Frac_all in comparison to CIC. In addition, the error on the X-axis were better in Frac_λμ compared to Frac_all, but this was not considered because the wall was placed on the Y-axis.

https://doi.org/10.1017/S0263574720001356 Published online by Cambridge University Press

Table VII. Contact force errors RMSE, MSE, and MAE, K_e =200 N/m.

	RMSE		MSE		MAE	
***Ke* =200 N/m**	***X***	***Y***	***X***	***Y***	***X***	***Y***
CIC	1.5968	1.5113	2.5499	2.2840	0.3387	0.4544
Frac_λμ	**1.4080**	1.1165	**1.9825**	1.2465	0.2078	0.3069
Frac_all	1.4489	**0.7977**	2.0992	**0.6363**	**0.1838**	**0.2199**

MSE, mean squared error; MAE, mean absolute error.

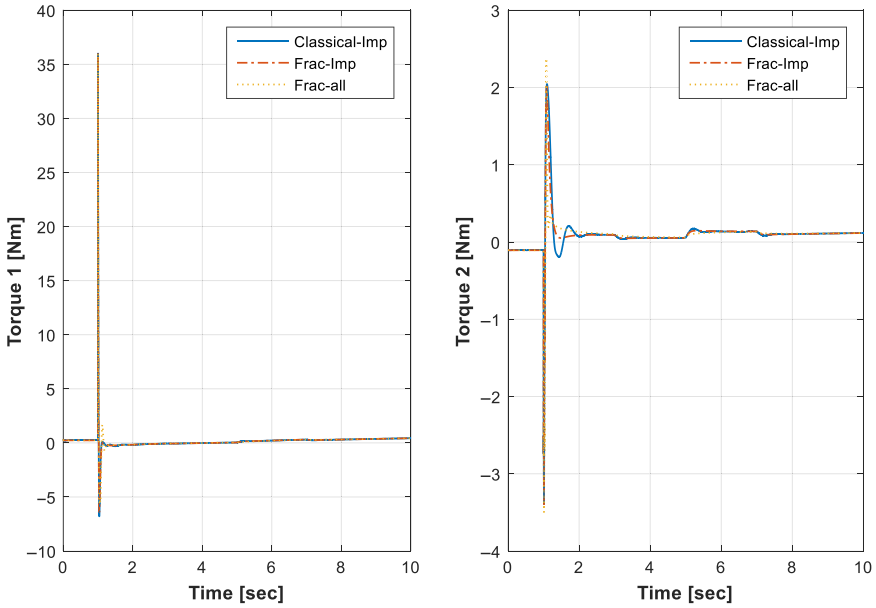

Fig. 13. Joint torques for the motion in Fig.12. Y_d= 180 mm, K_e= 200 N/m.

6. Conclusion

This paper introduced a novel FOIC method for improving the interaction forces between robots and their environments. Computer simulations were conducted on a RR type serial manipulator in which computed torque controller was used for the position control. All the parameters related to the FOIC and CIC were determined using the simplex search optimization algorithm. In order to examine the proposed FOIC, different environment stiffness values were used. In addition, the robustness of the FOIC was tested on a flat and triangular-shaped wall. Three different performance indices were used in the calculation of the contact force errors to compare the performances of the FOIC and CIC. Based on the simulation experiments, the proposed FOIC can achieve better impact absorption performance and show more robust behavior which allows to achieve wider range of the interaction control. Results showed that an improvement of 15.6% was achieved from CIC to Frac_λμ, and an improvement of 42.3% was achieved in Frac_all in comparison to CIC by reducing the contact forces. When the environmental conditions of contact had changed, an improvement of 26.12% was achieved from CIC to Frac_λμ and an improvement of 47.21% was achieved from CIC to Frac_all by reducing the contact forces.

References

1. G. Xiong, H. Chen, R. Zhang and F. Liang, "Robot-environment interaction control of a flexible joint light weight robot manipulator," *Int. J. Adv. Robot. Syst.* **9**(3), 76 (2012). https://doi.org/10.5772/51308.
2. N. Hogan, "Impedance Control: An Approach to Manipulation," *Proceedings American Control Conference* (IEEE, 1984) pp. 304–313. https://doi.org/10.23919/acc.1984.4788393.
3. G. Ferretti, G. A. Magnani, P. Rocco, F. Cecconello and G. Rossetti, "Impedance Control for Industrial robots," *Proceedings - IEEE International Conference on Robotics and Automation* (2000) pp. 4027–4032. https://doi.org/10.1109/robot.2000.845359.

https://doi.org/10.1017/S0263574720001356 Published online by Cambridge University Press

4. N. Hogan, "Impedance control: An approach to manipulation: Part I-theory," *J. Dyn. Syst. Measur. Control Trans. ASME* **107**(1), 1–7 (1985). https://doi.org/10.1115/1.3140702.
5. S. Oh, H. Woo and K. Kong, "Frequency-shaped impedance control for safe human-robot interaction in reference tracking application," *IEEE/ASME Trans. Mech.* **19**(6), 1907–1916 (2014). https://doi.org/10.1109/TMECH.2014.2309118.
6. S.-Y. Lo, C.-A. Cheng, H.-P. Huang, S.-Y. Lo, C.-A. Cheng and H.-P. Huang, "Virtual impedance control for safe human-robot interaction," *J. Intell. Robot. Syst.* **82**(1), 3–19 (2016). https://doi.org/10.1007/s10846-015-0250-y.
7. F. Lange, W. Bertleff and M. Suppa, "Force and Trajectory Control of Industrial Robots in Stiff Contact," *Proceedings - IEEE International Conference on Robotics and Automation* (2013) pp. 2927–2934. https://doi.org/10.1109/ICRA.2013.6630983.
8. B. Komati, M. R. Pac, I. Ranatunga, C. Clévy, D. O. Popa and P. Lutz, "Explicit Force Control vs Impedance Control for Micromanipulation," *Proceedings of ASME Design Engineering Technical Conferences* (2013) pp. 1–8. https://doi.org/10.1115/DETC2013-13067.
9. T. Haidegger, B. Benyö, L. Kovács and Z. Benyö, "Force sensing and force control for surgical robots," *IFAC Proceedings Volumes*, **7**(1), 401–406 (2009). https://doi.org/10.3182/20090812-3-DK-2006.0035.
10. S. Das, *Functional Fractional Calculus* (2011). https://doi.org/10.1007/978-3-642-20545-3.
11. I. Petráš, *Fractional-Order Feedback Control of A Dc Motor* (2009).
12. A. Dumlu, "Design of a fractional-order adaptive integral sliding mode controller for the trajectory tracking control of robot manipulators," *Proc. Inst. Mech. Eng. Part I J. Syst. Control Eng.* **232**(9), 1212–1229 (2018). https://doi.org/10.1177/0959651818778218.
13. Y. Q. Chen, I. Petráš and D. Xue, "Fractional Order Control - A Tutorial," *Proceedings of American Control Conference* (2009) pp. 1397–1411. https://doi.org/10.1109/ACC.2009.5160719.
14. M. Nakagava and K. Sorimachi, "Basic characteristics of a fractance device," *IEICE Trans. Fund.* **E75-A**(12), 1814–1818 (1992).
15. J. A. T. Machado and A. Azenha, "Fractional-Order Hybrid Control of Robot Manipulators," *Proceedings of IEEE International Conference on Systems, Man and Cybernetics* (IEEE, 1998) pp. 788–793. https://doi.org/10.1109/icsmc.1998.725510.
16. F. Hongmei, S. Yu and Z. Xiaobin, "Research on Fractional Order Controller in Servo Press Control System," *Proceedings of the 2007 IEEE International Conference on Mechatronics and Automation ICMA 2007* (2007) pp. 2934–2938. https://doi.org/10.1109/ICMA.2007.4304026.
17. S. Das and I. Pan, "Fractional Order System Identification," **In**: *SpringerBriefs in Applied Sciences and Technology* (Springer Verlag, 2012) pp. 67–81. https://doi.org/10.1007/978-3-642-23117-9_5.
18. I. Podlubny, "Fractional-order systems and PIλDμ-controllers," *IEEE Trans. Autom. Control* **44**(1), 208–214 (1999). https://doi.org/10.1109/9.739144.
19. P. Shah and S. Agashe, "Review of fractional PID controller," *Mechatronics* **38**, 29–41 (2016). https://doi.org/10.1016/j.mechatronics.2016.06.005.
20. S. Oh and Y. Hori, "Fractional Order Impedance Control by Particle Swarm Optimization," *2008 International Conference on Control, Automation and Systems ICCAS 2008* (2008) pp. 1936–1941. https://doi.org/10.1109/ICCAS.2008.4694414.
21. Y. Kobayashi, T. Ando, T. Watanabe, M. Seki and M. G. Fujie, "Fractional Impedance Control for Reproducing the Material Properties of Muscle," *IEEE/RSJ 2010 International Conference on Intelligent Robots and Systems, IROS 2010 - Conference Proceedings* (2010) pp. 5498–5504. https://doi.org/10.1109/IROS.2010.5650195.
22. Y. Chen, J. Zhao, J. Wang and D. Li, "Fractional-Order Impedance Control for a Wheel-Legged Robot," *Proceedings of the 29th Chinese Control and Decision Conference CCDC 2017* (2017) pp. 7845–7850. https://doi.org/10.1109/CCDC.2017.7978618.
23. J. de Gea and F. Kirchner, "Modelling and Simulation of Robot Arm Interaction Forces Using Impedance Control," *IFAC Proc.* **41**(2), 15589–15594 (2008). https://doi.org/10.3182/20080706-5-kr-1001.02636.
24. S. Kizir and A. Alshawi, "Impedance Control of 2dof Serial Robot Manipulator," *International Conference on Advanced Technologies, Computer Engineering and Science (ICATCES'18)*, vol. 1 (2018) pp. 244–249.
25. S. Kizir and Z. Bingül, "Fuzzy impedance and force control of a *Stewart platform," Turkish J. Electr. Eng. Comput. Sci.* **22**(4), 924–939 (2014). https://doi.org/10.3906/elk-1208-54.
26. D. Valério and J. Sá da Costa, "Ninteger: A Non-integer Control Toolbox for MatLab," *Proceedings of the First IFAC Workshop on Fractional Differentiation and Applications, Bordeaux, France* (2004) pp. 208–213.
27. J. C. Lagarias, J. A. Reeds, M. H. Wright and P. E. Wright, "Convergence properties of the Nelder-Mead simplex method in low dimensions," *SIAM J. Optim.* **9**(1), 112–147 (1998). https://doi.org/10.1137/S1052623496303470.
28. Y. Chen, J. Zhao, B. Wang and S. Han, "High Precision Fuzzy Impedance Control of Free-Form Surfaces Polishing Robotic Arm Based on Position Control," *International Conference on Advanced Intelligent Mechatronics, AIM* (2005) pp. 819–824. https://doi.org/10.1109/aim.2005.1511084.
29. M. Benady, T. Flash and D. Gershon, *Robot Learning of Contact Tasks* (North Holland, Amsterdam, 1990) pp. 147–159.